Electronic Supplementary Material (ESI) for Journal of Materials Chemistry A.

Supporting Information

Conductivity-controllable Rubber Films Responsive to Humidity Based on Bio-based Continuous Segregated Cell Network

Xinghuo Wang, Chuanhui Xu, Qi Shen, Mengzhuan Lin, Zhongjie Zheng, Baofeng Lin, Lihua Fu*

School of Chemistry and Chemical Engineering, Guangxi University, Nanning 530004, China

Corresponding Author: Chuanhui Xu xuhuiyee@gxu.edu.cn

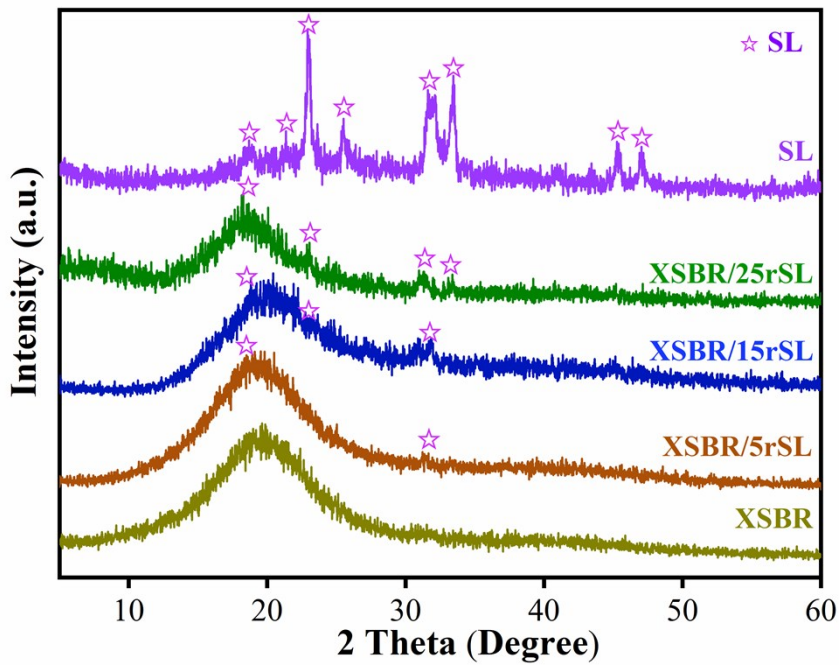

Figure S1. XRD curves of SL, XSBR and XSBR/rSL.

The existence of rSL was confirmed by XRD analysis. As shown in Figure S1, the 2θ = 19.9 º, 21.9 º, 24.6 º, 29.9 º, 32.1 º, 33.1 º, 44.5 º, and 48.7 º were well consistent with those of SL reported by Liu et al[1]. The diffraction peaks at 2θ = 19.9 º, 24.6 º, 32.1 º, and 33.1 º shown in the spectrum of XSBR/rSL films demonstrate that the SL molecules were adsorbed and deposited in the composites effectively. The crystallization peaks of SL can be seen in films, that is, SL has been regenerated in the films. (Regeneration process refers to: SL powder was first dissolved in 100 ml water to form a solution, and then mixed with 20 g latex solution and stirred evenly, the SL molecules oriented and entangled mutually under the "capillary force", which finally precipitated from solution and filled in

the interstitial "channels" between XSBR latex particles and form isolation network during film-formation.) Additionally, for neat XSBR, a wide hump appeared at about 20 ° which was a typical diffraction peak of amorphous polymers[2]. The result proves that SL is successfully regenerated in the XSBR rubber matrix during the formation of films.

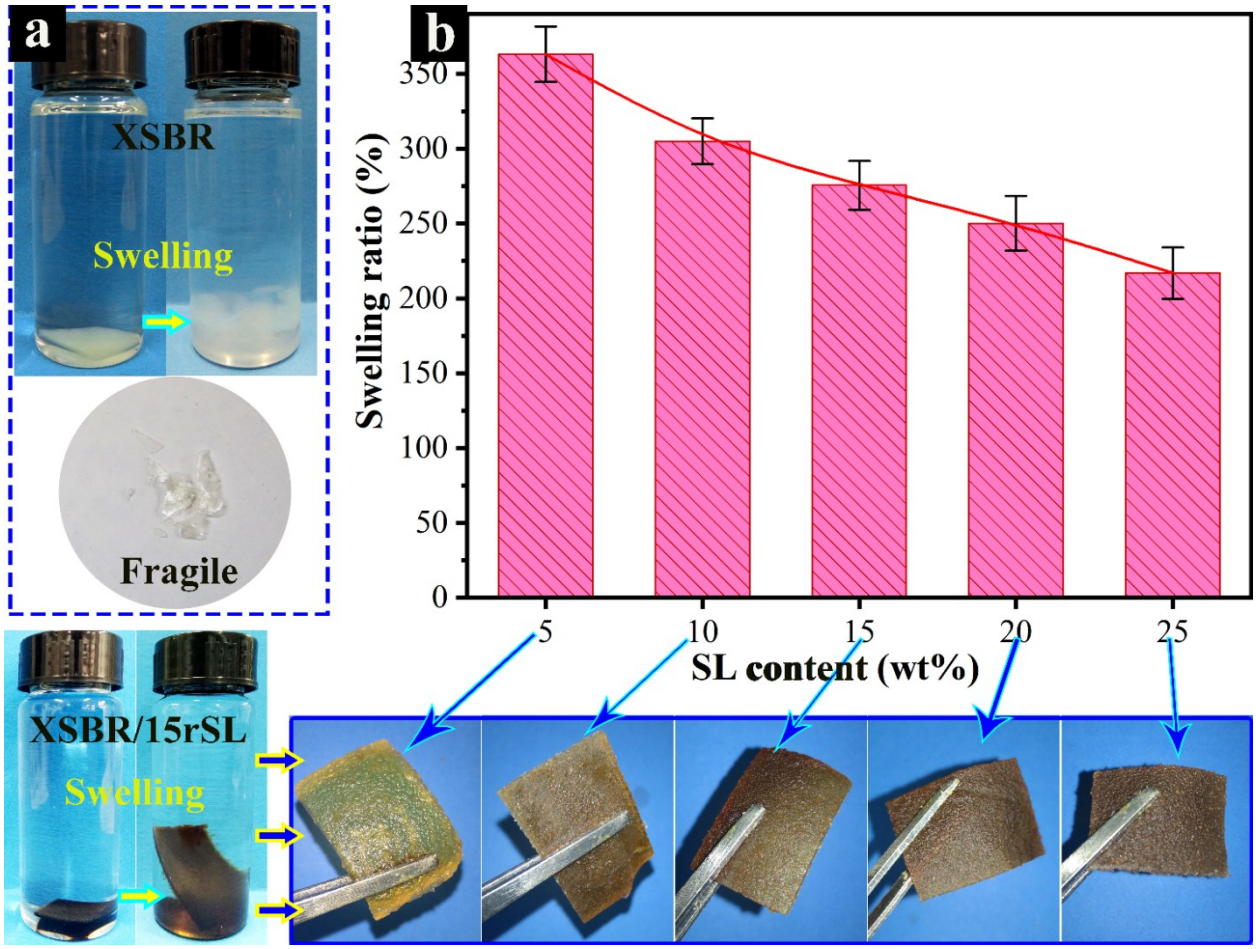

Figure S2. a) photographs of samples before and after the swelling in toluene for 72 h. b) The swelling ratio of XSBR/rSL films.

The consequences of equilibrium swelling experiments further elucidate the rSL network structure and its interaction with the XSBR matrix. As illustrated in Figure S2a, the swelled pure XSBR was completely brittle without any strength after soaking in toluene for 3 days. On the

contrary, all the films were just swollen in the toluene and the soaked samples remained intact perfectly, which confirmed that the continuous network formed by rSL penetrated through the whole uncrosslinked rubber matrix (Figure 2, TEM images) and avoided fragmentation. Furthermore, the toluene absorption rate of the films gradually decreased with the increase of rSL contents. As shown in Figure S2b, the swelling ratio decreased from 363 to 217 % with the content of rSL increasing from 5 to 25 wt%. The consequence demonstrates that the interaction between rSL and XSBR limited the movement of XSBR chains, which significantly ameliorated the solvent resistance of the films[3]. One side, it should be emphasized that the formation of a continuous network provides the possibility for the application of rubber films in the field of electrical conductivity. On the other hand, the interaction between filler and the rubber matrix is also essential to the solvent resistance of the films.

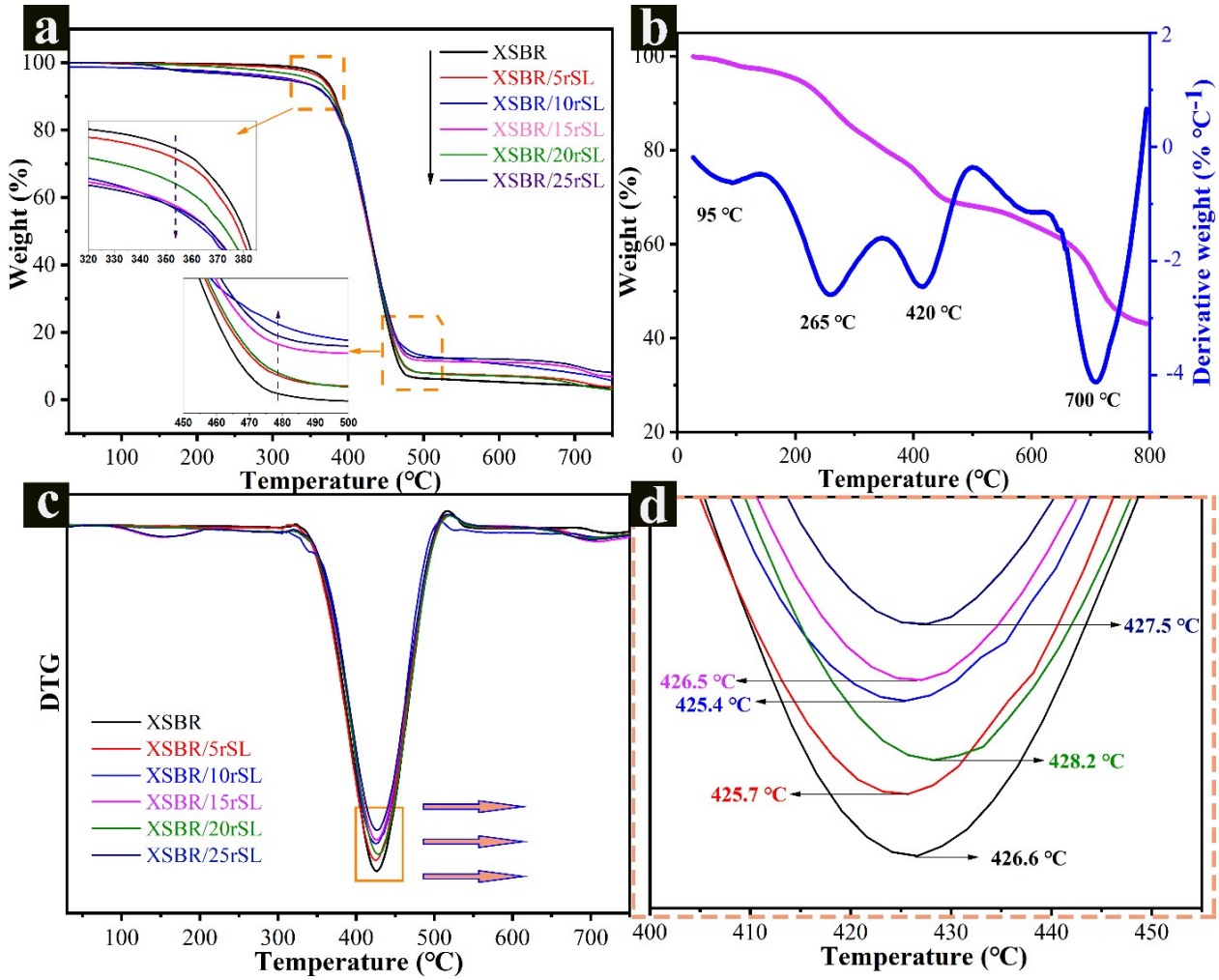

Figure S3. Thermogravimetric Analysis (TGA) and Micro quotient Thermogravimetry (DTG) curves of a, c, d) XSBR, XSBR/rSL and b) SL.

As shown in Figure S3a, four main weight loss steps are observed for the XSBR/rSL, suggesting a multi-decomposition process[4]. This is consistent with the thermal decomposition process of SL (Figure S3b). It can be noted from Figure S3c and d that the maximum thermal decomposition temperatures of the samples with 5 and 10 wt% SL are 425.4 and 425.6 ℃ respectively, lower than 426.6 ℃ of XSBR. This result indicates that the hydrogen bond between XSBR and rSL is not quite strong. Similar results are presented in Huang's report, in which an emamectin benzoate-loaded alginate/chitosan/sodium lignosulfonate (EB-loaded ALG/CS/SL) polyelectrolyte was self-assembled via electrostatic interaction[5]. However, with further increase of SL content, the thermal

stability of the rubber film was improved. As seen, the maximum thermal decomposition temperature of XSBR/15rSL and XSBR/20rSL are 426.5 and 428.2 ℃, respectively. These consequences display that the formation of perfect segregated cell network had a positive effect on the thermal stability of the rubber film.

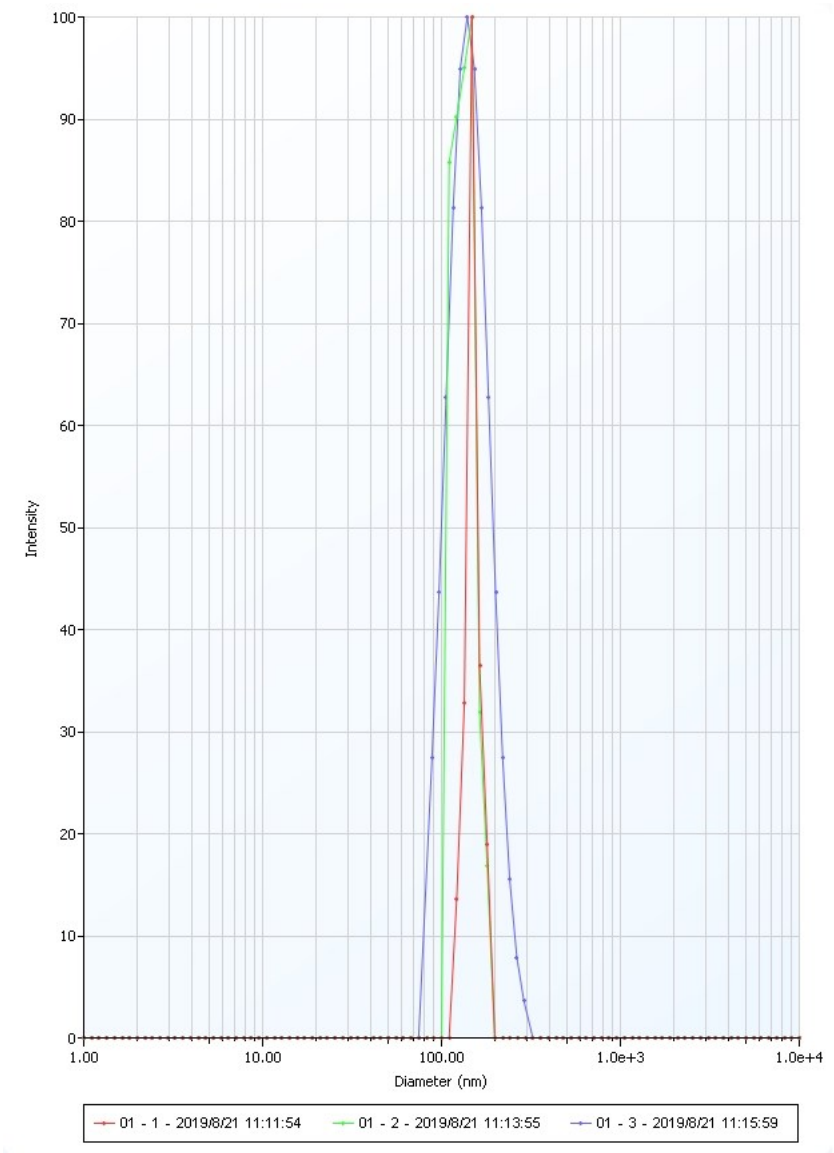

Figure S4. The chart of particle size of XSBR latex.

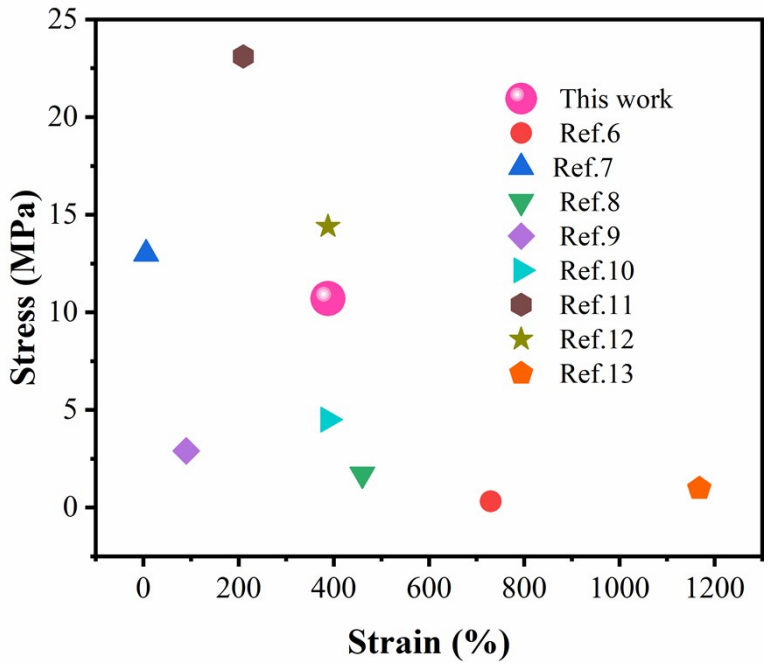

Figure S5. Comparison of tensile strength between our rubber film and other reported rubber materials with organized conductive network.

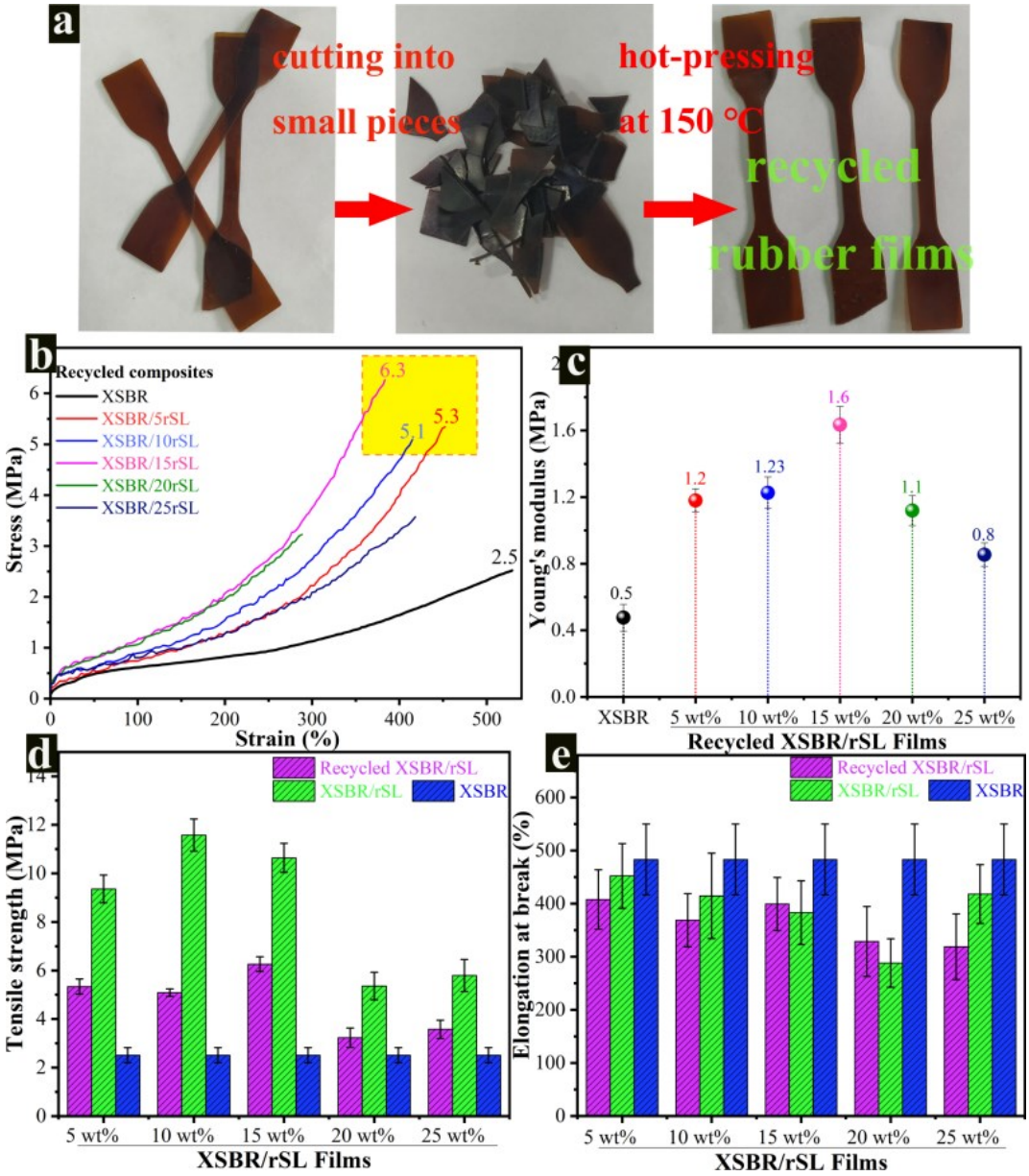

Figure S6. a) XSBR/ rSL films were cut into small pieces and then hot pressed to form new films. b) Stress-strain curves and c) Young's modulus of XSBR and recycled XSBR/rSL films. d) Tensile strength and d) elongation at break of neat XSBR, XSBR/rSL and recycled XSBR/rSL films.

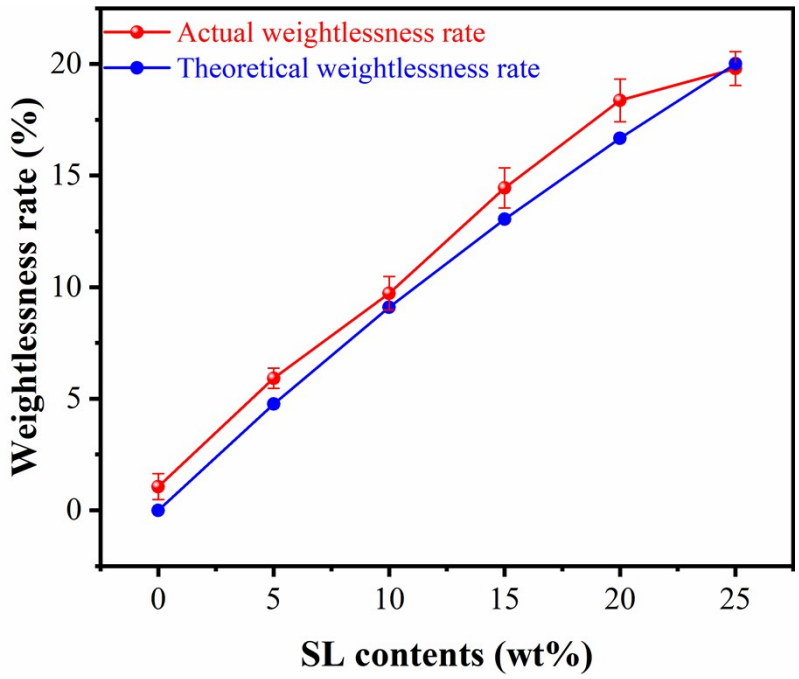

Figure S7. Weight loss rate of XSBR/rSL films with different SL contents after soaking in water for 3 days.

The calculation method of weight loss rate is as follows: firstly, the slurry film is dried in 60 oven for 8 hours, then the weight is measured (m_0), the film is soaked in deionized water solution for 3 days to remove water, and then put into the oven for drying for 12 hours to get m_1. The weight loss rate is: $\frac{m_0 - m_1}{m_0} \times 100\%$. When XSBR/rSL films with different SL content were immersed in water for 3 days, we found that the weight loss rate of the films was basically equal to the sum of SL content and impurities in pure XSBR film. That is, through soaking treatment, we can easily remove the biological isolation network and further recover the rubber matrix.

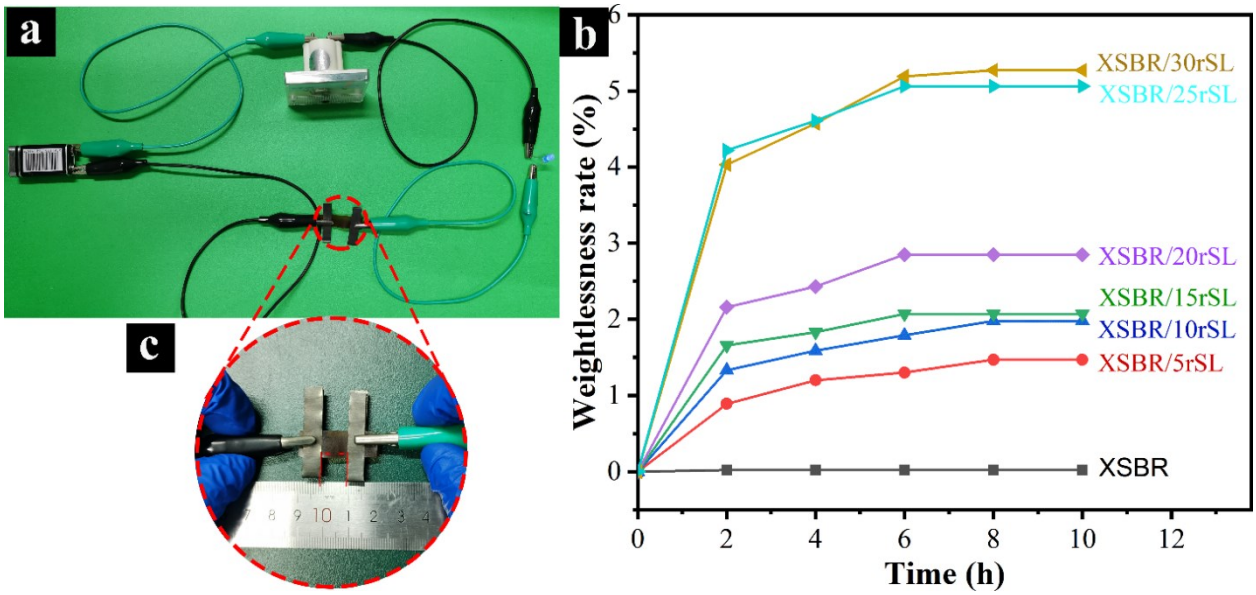

Figure S8. a) Physical diagram of test circuit. b) Weight loss rate of different samples dried in 60 ℃ oven for 10 h. c) Physical picture of test sample.

Due to the presence of bound water in the ordered rSL nanometer network structure, it is difficult to completely remove the water in the film[15,16]. To facilitate the clarity of expression in subsequent experiments, composites were put into a drying oven at 60 ℃ for continuous heating and drying. The consequence is shown in Figure S6b that the weight loss rate of all composites remains basically unchanged after continuous drying at 60 ℃ for 8 h. For the convenience of the description of the follow-up test process, we set the relative moisture content of the sample dried in 60 ℃ oven for 12 h as 0 %. Additionally, the sample was clamped by the metal clamp with excellent conductivity, and the conductivity test area was controlled at 10 (length) × 10 (width) × 1 (thickness) mm to ensure the accuracy of test comparison between different samples. Based on the applied voltage and obtained current, the resistivity across the conductive rubber composite was estimated for the different fabrication procedures of the electrode.

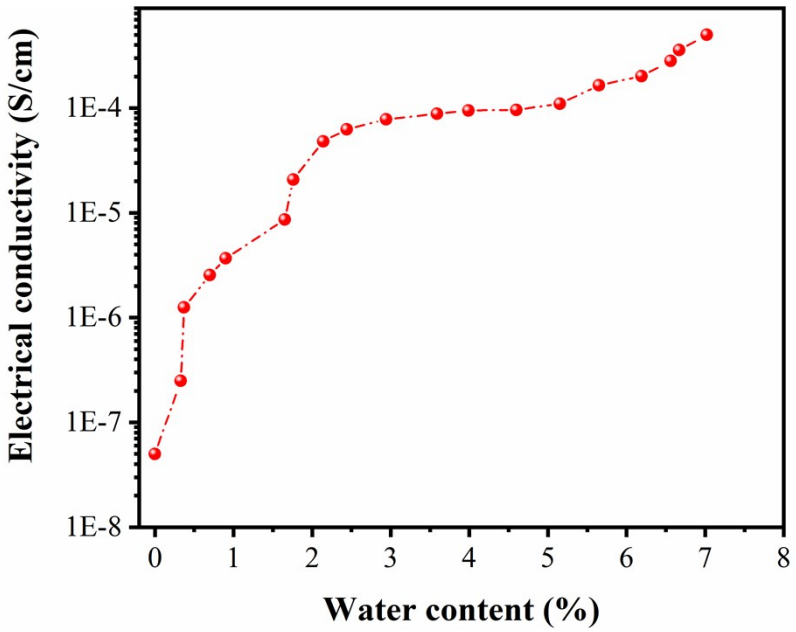

Figure S9. The effect of water content on the volume conductivity of conductive film.

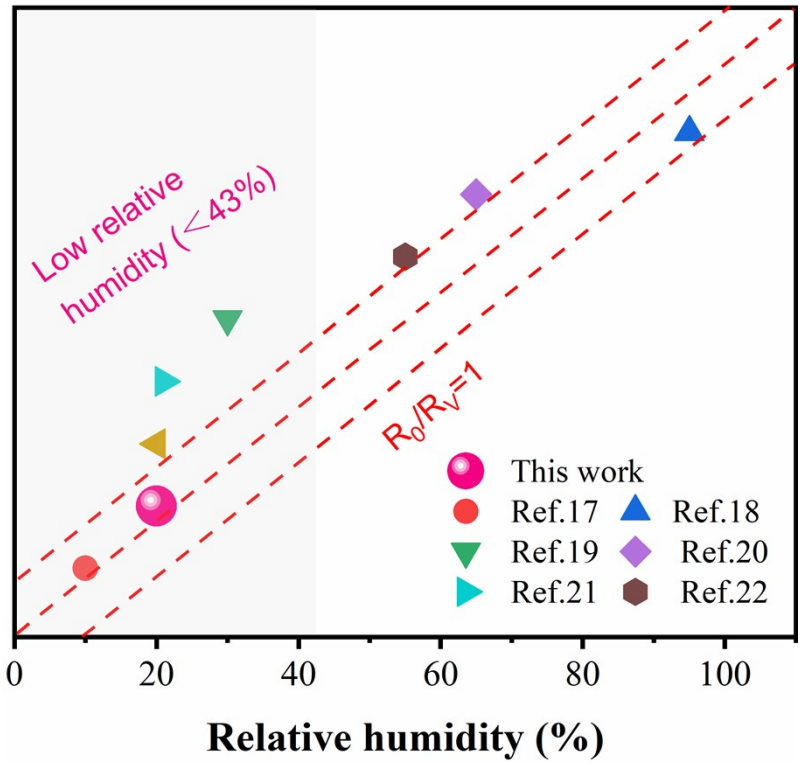

Figure S10. The minimum sensitivity of our rubber film to relative humidity was compared with other reported humidity sensors.

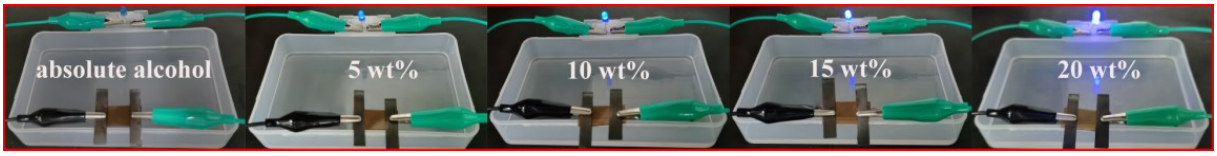

Figure S11. Conducting experiments for the samples soaking in the ethanol/aqueous mixture with water content of 0, 5, 10, 15, and 20 wt% after 2 min.

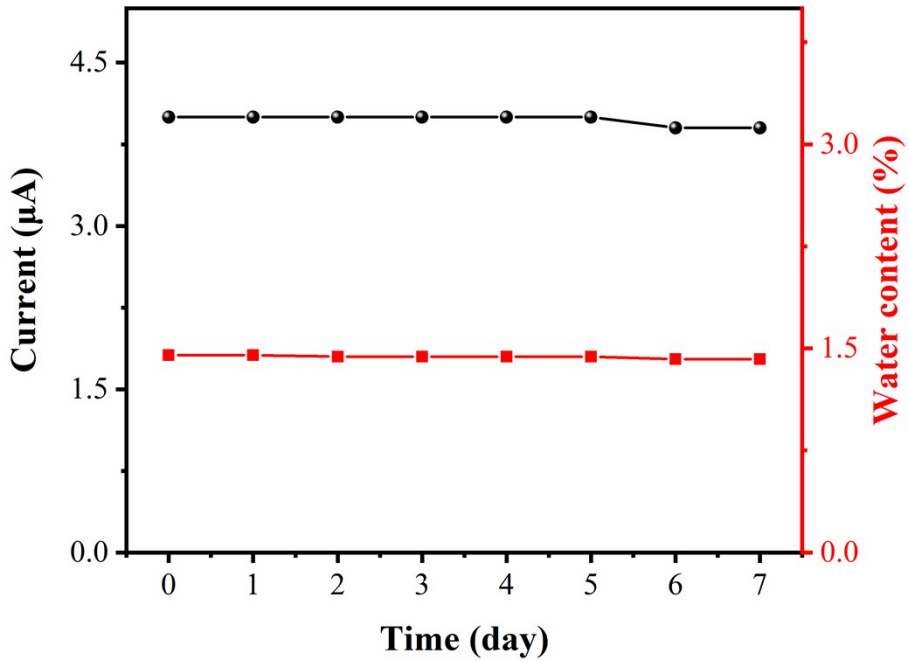

Figure S12. The water content and current of the rubber film wrapped by PE film change with time.

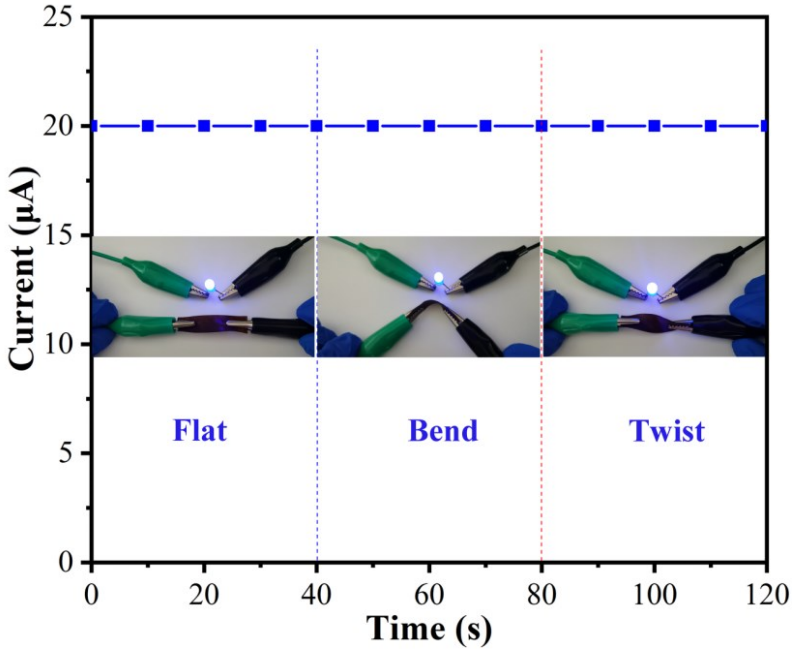

Figure S13. The demonstration of conductivity stability of the film (water content 2.1 %) under various non-stretching deformations.

1 M. Liu, C. Zhang, B. Hu, Z. Sun, Q. Xu, J. Wen, J. Xiao, Y. Dong, M. Gan, W. Sun, J. Zhu, D. Chen, *Appl. Surf. Sci.* 2020, **507**.

2 W. Wu, C. Xu, Z. Zheng, B. Lin, L. Fu, *J. Mater. Chem. A* 2019, **7**, 6901.

3 S. Xiao, Y. Tan, J. Xu, C. Xiong, X. Wang, S. Su, *Appl. Clay Sci.* 2014, **97-98**, 91.

4 J. Pang, W. Zhang, H. Zhang, J. Zhang, H. Zhang, G. Cao, M. Han, Y. Yang, *Carbon* 2018, **132**, 280.

5 G. Huang, G. Qian, Y. Yan, D. Xu, C. Xu, L. Fu, B. Lin, *React. Funct. Polym.* 2020, **146**.

6. X. Yang, J. Z. Liu, D. Y. Fan, J. Cao, X. Huang, Z. Zheng and X. X. Zhang, *Chem. Eng. J.*, 2020, 389.

7. X. Y. Qiu, Q. Q. Guo, Y. Y. Wang, X. Huang, J. Cao, Z. Zheng and X. X. Zhang, *Acs Appl. Mater. Inter.*, 2020, 12, 41981-41990.

8. Y. M. Tang, Q. Q. Guo, Z. M. Chen, X. X. Zhang, C. H. Lu, J. Cao and Z. Zheng, *Acs Appl. Mater. Inter.*, 2019, 11, 23527-23534.

9. J. Cao, C. L. Zhou, G. H. Su, X. X. Zhang, T. Zhou, Z. H. Zhou and Y. B. Yang, *Adv. Mater.*, 2019, 31.

10. Q. Q. Guo, Y. Y. Luo, J. Z. Liu, X. X. Zhang and C. H. Lu, *J. Mater. Chem. C*, 2018, 6, 2139-2147.

11. J. Huang, X. Zhao, Y. Wu, N. Yang, C. Ma, Y. Cheng and J. Zhang, *Carbon*, 2021, 173, 667-675.

12. X. Huang, Q. Q. Guo, P. Zhou, C. H. Lu, G. P. Yuan, Z. M. Chen and X. X. Zhang, *Compos. Part B-Engineering*, 2020, 182.

13. X. H. Liu, G. H. Su, Q. Q. Guo, C. H. Lu, T. Zhou, C. L. Zhou and X. X. Zhang, *Adv. Funct. Mater.*, 2018, 28.

14. J. Yang, X. An, L. Liu, F. T. Seta, H. Zhang, S. Nie, S. Yao, H. Cao, Q. Xu, H. Liu, Y. Ni, *Cellulose* 2020, **27**, 5071;

15. H. Liu, Q.-d. An, J. Kim, L. Guo, Y.-m. Zhao, Z.-y. Xiao, S.-r. Zhai, *J. Hazard. Mater.* 2020, **391**.

16. D. Wang, Y. Huang, W. Cai, M. Tian, P. Liu and Y. Zhang, *J. Appl. Polymer Sci.*, 2014, **131**, n/a-n/a.

17. Y. Chen, J. Nie, C. Xu, W. Wu and Z. Zheng, *ACS Sustain. Chem. Eng.*, 2019, **8**, 1285-1294.

18. Elham Davoodi, Hossein Montazerian, Reihaneh Haghniaz, Armin Rashidi, Samad Ahadian, Amir Sheikhi, Jun Chen, Ali Khademhosseini, Abbas S. Milani, Mina Hoorfar, and Ehsan Toyserkani. *ACS Nano*, 2020, **14**, 1520−1532

19. W. Huang, J. Li, D. Liu, S. Tan, P. Zhang, L. Zhu and S. Yang, *ACS Appl. Polymer Mater.*, 2020, **2**, 2119-2125.

20. H. Montazerian, A. Rashidi, A. Dalili, H. Najjaran, A. S. Milani and M. Hoorfar, *Small*, 2019, **15**.

21. Y. Guan, Y. Song, H. Li, L. Ye, B. Lu, J. Zang and Y. Yu, *J. Mater. Chem. C*, 2019, **7**, 2853-2864.

22. M. Nankali, N. M. Nouri, M. Navidbakhsh, N. G. Malek, M. A. Amindehghan, A. M. Shahtoori, M. Karimi and M. Amjadi, *J. Mater. Chem. C*, 2020, **8**, 6185-6195.